Molecular Therapy
Oncolytics
Original Article

Gene Silencing of Transferrin-1 Receptor as a Potential Therapeutic Target for Human Follicular and Anaplastic Thyroid Cancer

Agata Campisi,[1] Roberta Bonfanti,[1] Giuseppina Raciti,[1] Gabriele Bonaventura,[2] Laura Legnani,[1] Gaetano Magro,[3] Marzio Pennisi,[1] Giulia Russo,[1] Maria Assunta Chiacchio,[1] Francesco Pappalardo,[1] and Rosalba Parenti[4]

[1]Department of Drug Sciences, University of Catania, Viale A. Doria 6, 95125 Catania, Italy; [2]Institute for Biomedical Research and Innovation (IRIB), Italian National Research Council, Via P. Gaifami 18, 95126 Catania, Italy; [3]Department of Department of Medical, Surgical, and Technological Sciences "G.B. Ingrassia," University of Catania, Via S. Sofia 87, 95123 Catania, Italy; [4]Department of Biomedical and Biotechnological Sciences, University of Catania, Via S. Sofia 97, 95123 Catania, Italy

Herein, we assess the gene expression changes activated in thyroid tumors through a computational approach, using the MapReduce algorithm. Through this predictive analysis, we identified the TfR1 gene as a critical mediator of thyroid tumor progression. Then, we investigated the effect of TfR1 gene silencing through small interfering RNA (siRNA) in the expression of extracellular signal-regulated kinase 1/2 (Erk1/2) pathway and c-Myc in human differentiated follicular and undifferentiated anaplastic thyroid cancer. The expression levels of cyclin D_1, p53, and p27, proteins involved in cell cycle progression, were also evaluated. The effect of TfR1 gene silencing through siRNA on the apoptotic pathway activation was also tested. Computational prediction and *in vitro* studies demonstrate that TfR1 plays a key role in thyroid cancer and that its downregulation was able to inhibit the ERK pathway, reducing also c-Myc expression, which blocks the cell cycle and activates the apoptotic pathway. We demonstrate that TfR1 plays a crucial role for a rapid and transient activation of the ERK signaling pathway, which induces a deregulation of genes involved in the aberrant accumulation of intracellular free iron and in drug resistance. We also suggest that TfR1 might represent an important target for thyroid cancer therapy.

INTRODUCTION

Thyroid cancer is one of the most common endocrine tumors, classified as either differentiated or undifferentiated cancer. Differentiated cancers include papillary and follicular thyroid carcinoma, while undifferentiated types include medullary thyroid and anaplastic cancers. In particular, follicular thyroid cancer represents the second most prevalent type, and it accounts for 10%–15% of all thyroid cancer. In contrast, anaplastic thyroid cancer is rare, but extremely aggressive, contributing up to 30%–40% of thyroid cancer-specific mortality.

Several studies have provided experimental support for anticancer therapies using as a target transferrin receptor (TfR1 or CD71).[1–3] TfR1 is a transmembrane receptor structurally characterized by a dimer of two identical subunits (disulfide linked) capable of binding diferric transferrin and delivering it into the cell cytosol.[4–7] TfR1 expression is mediated by the need of cells for iron and is largely expressed in different areas of the human body.[8,9] The molecular mechanism that drives regulation of TfR1 gene expression is mediated in the cytoplasm through specific mRNA protein interactions at the post-transcriptional level.[10] The 3′ untranslated region of receptor mRNA contains a series of five hairpin stem-loop structures required for iron-dependent regulation. The stem-loop structures, called iron-responsive elements (IREs), are recognized by *trans*-acting proteins, known as iron-regulatory proteins (IRPs), that control the rate of mRNA translation or stability.[11,12] Signals other than iron levels, such as nitric oxide and oxidative stress, can also regulate IRPs and modulate cellular iron metabolism.[9,13–16] The expression of TfR1 is also regulated by the status of cellular proliferation[17,18] that could be mediated by mitogens, which are able to modulate various protein kinase activities through either the activation of gene transcription or the stabilization of mRNA.[19]

The Ras/Raf/mitogen-activated protein kinase kinase (MEK)/extracellular signal-regulated kinase (ERK) signaling pathway can exert proliferative or anti-proliferative effects through downstream transcription factor targets, including nuclear factor κB (NF-κB), cyclic AMP response element binding protein (CREB), Ets-1, activator protein 1 (AP-1), and c-Myc. ERK1/2 can directly phosphorylate Ets-1, AP-1, and c-Myc, which leads to their activation. Alternatively, ERK1/2 can phosphorylate and activate a downstream kinase target, RSK, which then phosphorylates and activates transcription factors, such as CREB. These transcription factors induce the expression of genes important for cell cycle progression, such as cyclin-dependent kinases, cyclins, growth factors, and apoptosis prevention. However, under certain circumstances, strong Raf signaling has been shown to result in the inactivation of downstream transcription factors, including c-Myc, which may account for the Raf-induced anti-proliferative

Received 13 July 2019; accepted 9 January 2020;
https://doi.org/10.1016/j.omto.2020.01.003.

Correspondence: Agata Campisi, PhD, Department of Drug Sciences, University of Catania, Viale A. Doria 6, 95125 Catania, Italy.
E-mail: campisag@unict.it

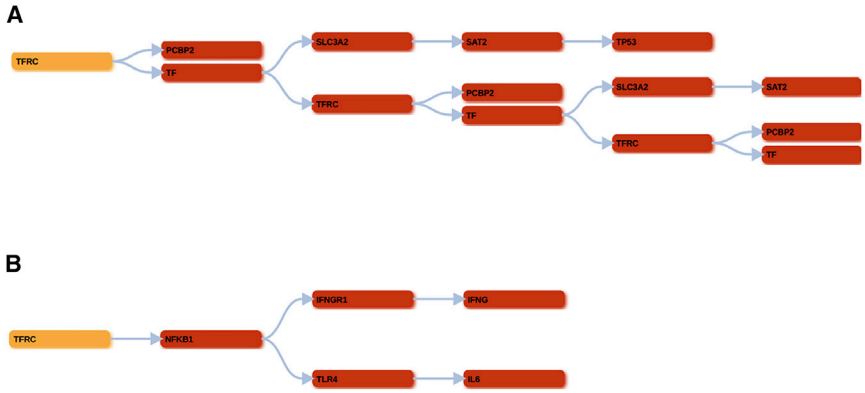

Figure 1. *In Silico* Studies to Search Target Nodes to Modulate TfR1

(A) The TFRC output tree obtained by executing the algorithm on 5 hops and on the ferroptosis pathway (hsa04216). (B) The TFRC output tree obtained by executing the algorithm on 5 hops and on the HIF-1 signaling pathway (hsa04066).

responses observed in cancers. TfR1 is a direct transcriptional target of the c-Myc proto-oncogene, one of the most frequent proteins in human malignancies, that is necessary for cellular proliferation and promotes tumorigenesis.[20–24]

Currently, computational modeling and *in silico* simulations represent helpful resources for the prediction and optimization of specific and potential interventions against cancers. Existing works on several computational approaches have sought to improve knowledge about cancer modulation and chemosensitivity in target therapy.[25,26]

In this study, we addressed the gene expression changes activated in thyroid tumors through a computational approach, using the MapReduce algorithm.[27] Through this analysis, we identified the TfR1 gene as a critical mediator of thyroid tumor progression. Therefore, we investigated the effect of TfR1 gene silencing through small interfering RNA (siRNA) in a human carcinoma follicular cell line (FTC-133) and a human anaplastic cell line (8305C). In addition, the ERK1/2 pathway and c-Myc expression levels were analyzed. The expression levels of cyclin D_1, p53, and p27, proteins involved in cell cycle progression, were also assessed. The effects of TfR1 gene silencing through siRNA on cellular viability, cell growth, and apoptotic pathway activation were also tested.

RESULTS

In Silico Studies to Search Target Nodes to Modulate TfR1

To discover any potential candidate targets involved in the progression of thyroid cancer or in the acquired drug resistance phenomena, we ran the MapReduce algorithm on TfR1 pathway activation, also called the ferroptosis pathway (hsa04216), using as a target node the TFRC (hsa7037) gene that belongs to the TfR1 receptor according to Kyoto Encyclopedia of Genes and Genomes (KEGG) nomenclature. The resulting tree is shown in Figure 1. We recall here that the TFRC gene is modulated by two arms represented by TF and PCBP2, respectively. TF is fundamental for the binding and associated protein interaction with TFRC, while PCBP2 is connected with TFRC through a protein-compound interaction. The depth of the search (hop value) was set to 5. After the launch of the software, we obtained a generation of 11 neighbor genes for TF and none for PCBP2, for a total of 11 S-level ancestor genes. In the TF arm, the output graph pointed out the presence of the TP53 gene, also known as p53, as one of the possible neighbor genes involved in the modulation of the signaling pathway of TfR1, which plays an important role of transcription factor and target gene product. Furthermore, we assessed, through the "calculate occurrence" panel, the number of times that the ferroptosis pathway has been found in all of the pathways downloaded from KEGG during the research process, between the starting gene (TFRC) and the ending gene (TP53). Toward this aim, 256 occurrences were detected of the following pathway: TFRC → TF → SLC3A2 → SAT2 → TP53 (Figure 1A). Since TfR1 is connected to the hypoxia-inducible factor-1 (HIF-1) signaling pathway (hsa04066), we ran the algorithm using as target node TFRC (hsa7037) and a hop value equal to 5 for the depth of the search. As reported in Figure 1B, we found that the TFRC gene is modulated by NF-κB signaling, which plays a fundamental downstream transcription factor target of the Ras/Raf/MEK/ERK pathway. After the run of the software, we obtained a generation of four neighbor genes for NF-κB. Through the calculate occurrence panel, we calculated the number of times that the HIF-1 signaling pathway has been found in all of the pathways downloaded from KEGG during the search process, between the starting gene (TFRC) and the ending gene (NFKB1). To this purpose, five occurrences were detected and, in particular, the panel reported the following occurrences: (1) TFRC → NFKB1 → TLR4; (2) TFRC → NFKB1 → TLR4 → IL6; (3) TFRC → NFKB1; (4) TFRC → NFKB1 → IFNGR1; and (5) TFRC → NFKB1 → IFNGR1 → IFNG.

Computational results highlight the pivotal role of TP53 and NF-κB in the modulation of TfR1 expression and in the regulation of cell proliferative processes, respectively, suggesting the importance of silencing TfR1 gene expression.

Effect of the TfR1 Silencing Gene on Cellular Viability and Cell Growth

To validate *in silico* studies, FTC-133 and 8305C cell lines were transfected with the following siRNA: 5′-AACTTCAAGGTTTCTG CCAGC-3′. To choose the optimal concentration and the optimal transfection time of the cultures, the percentage of cellular viability through an MTT (3-(4,5-dimethylthiazol-2-yl)-2,5-dimethyltetrazolium bromide) test was performed. FTC-133 and 8305C human thyroid cell line cultures were transfected with different concentrations of siRNA-TfR1 (2–10 nM) and scrambled siRNA, used as a control,[22] for 24, 48, and 72 h. We found that the better concentration of

Table 1. Effect of RNA Interference on the Percentage of Cell Viability in FTC-133 Cells

Treatment	% of Inhibition of Cell Viability		
	24 h	**48 h**	**72 h**
2 nM scrambled	99.01 ± 1	98.77 ± 1	99.31 ± 1
4 nM scrambled	98.97 ± 2	97.89 ± 2	98.72 ± 2
6 nM scrambled	98.45 ± 2	98.34 ± 3	97.44 ± 2
8 nM scrambled	97.86 ± 3	98.78 ± 2	99.33 ± 1
10 nM scrambled	97.93 ± 2	97.88 ± 2	97.01 ± 2
2 nM siRNA	94.99 ± 1	91.01 ± 1	89.58 ± 3
4 nM siRNA	86.78 ± 1*	83.06 ± 3*	81.99 ± 1*
6 nM siRNA	78.67 ± 3*	66.78 ± 2*	65.97 ± 2*
8 nM siRNA	70.24 ± 2*	51.55 ± 1*	51.34 ± 1*
10 nM siRNA	64.01 ± 2*	42.88 ± 3*	41.99 ± 2*

The effect of RNA interference on the percentage of cell viability was determined though an MTT test in human follicular human thyroid cancer cell line cultures (FTC-133) transfected with different concentrations (2, 4, 6, 8, and 10 nM) of scrambled control or siRNA-TfR1 for 24, 48, and 72 h. Results are expressed as the mean ± SD of the values of five separate experiments performed in triplicate. *$p < 0.05$ for differences versus controls.

siRNA-TfR1 to transfect cell line cultures was 10 nM for 48 h (Tables 1 and 2). The effects of 10 mM siRNA-TfR1 transfection for 24, 48, and 72 h in both cell line cultures were also examined by using a growth curve constructed through trypan blue staining (Figure 2). In scrambled FTC-133 (Figure 2A) and 8305C (Figure 2C) cell line cultures, a rapidly significant increase of cell growth curve from 24 and 72 h was found. A progressive reduction in cellular proliferation in FTC-133- and 8305C-transfected cells with 10 nM siRNA-TfR1 was observed, when compared with the respective scrambled ones. Phase-contrast microscopy showed morphological changes in siRNA-TfR1-transfected cell line cultures. The cells appeared to progressively lose their characteristics (Figures 2B and 2D). In particular, following transfection for 48 h, the irregular changes in morphology increased, including shrinkage of the cell membranes and apoptotic cells, when compared with the respective control. The effect was more evident in FTC-133 cell line cultures. Thus, the subsequent experiments cells were transfected by using 10 nM siRNA-TfR1 for 48 h.

Effect of the TfR1 Silencing Gene on TfR1 Expression Levels

To verify whether siRNA transfection was able to inhibit mRNA for TfR1 in FTC-133 and 8305C cell line cultures, RT-PCR semiquantitative analysis was performed. A significant inhibition in the mRNA expression for TfR1 in both cell line cultures was observed, when compared with the respective scrambled ones, used as controls (Figures 3A and 3B). Furthermore, we assessed through immunofluorescence on single cells and western blot analysis on total cellular lysates the expression levels of TfR1 in FTC-133 and 8305C cell line cultures. A significant reduction of positive cells for TfR1 in FTC-133 (Figure 4Ab) and 8305C (Figure 4Bd) was found when compared with the respective scrambled-transfected ones (Figures 4Aa and 4Bc).

No non-specific staining was observed for TfR1 in cell cultures in which the primary antibody was omitted. Immunoblots and densitometric analysis performed on total cellular lysates obtained after siRNA transfection highlighted a significant reduction of TfR1 expression levels both in FTC-133 and 8305C cell line cultures, when compared with the scrambled ones (Figures 4C and 4D).

These results demonstrate that siRNA transfection induced the silencing of TFR1 gene expression in FTC-133 and 8305C human thyroid cancer cell lines.

Effect of TfR1 Gene Silencing on the ERK1/2 Pathway

ERK1/2 protein expression levels were detected in total cellular lysates through western blot analysis from both scrambled and 10 nM siRNA-TfR1-transfected FTC-133 and 8305C cell line cultures for 48 h (Figure 5). Immunoblots and densitometric analysis showed that siRNA-TfR1 transfection induced a significant reduction of ERK2 expression levels (Figures 5A and 5C) in both cell lines, when compared with the ERK1 expression levels (Figure 5B) and the respective scrambled ones (Figures 5A–5C). Furthermore, since TfR1 in thyroid-derived cell lines could be considered as an activator of the oncogene c-Myc, we evaluated in the same experimental conditions the expression of this gene. TfR1 gene silencing was able to reduce c-Myc expression levels in FTC-133 and 8305C cell lines, when compared with the respective scrambled-treated ones (Figures 5C and 5D). The effect on ERK1/2 and c-Myc expression levels appeared more evident in FTC-133-transfected cells. Densitometric analysis demonstrates that siRNA-TfR1 silencing induced a significant reduction of c-Myc expression levels in FTC-133 and 8305C cell line cultures, when compared with the scrambled ones (Figure 5D).

These experiments demonstrate that the gene silencing of TfR1 was able to inhibit ERK2 and c-Myc expression levels in FTC-133 and 8305C cell line cultures and that the effect appeared more evident in the FTC-133 cell line.

Effect of the TfR1 Silencing Gene on p53, p27, and Cyclin D_1 Expression Levels

To verify the effect of TfR1 downregulation on cell cycle regulator protein, the expression levels of the proteins involved in cell cycle (p53, p27, and cyclin D_1) were assessed. Figure 6 shows representative immunoblots and densitometric analysis for p53, p27, and cyclin D_1 expression levels detected in FTC-133 and 8305C thyroid cancer cells in scrambled and siRNA-TfR1-transfected cells. A significant increase of p27 and p53 expression levels was observed when compared with the respective scrambled-treated ones. Furthermore, we found that the expression of cyclin D_1 was at low levels in siRNA-transfected cell line cultures (Figures 6A and 6B). All of the effects were more evident in FTC-133 cell line cultures. These results demonstrate that the TfR1 silencing gene with siRNA leads to a block of cell cycle progression in both human thyroid cancer cell lines.

Table 2. Effect of RNA Interference on the Percentage of Cell Viability for 8305C Cells

Treatment	% of Inhibition of Cell Viability		
	24 h	**48 h**	**72 h**
2 nM scrambled	98.91 ± 1	99.01 ± 1	97.96 ± 2
4 nM scrambled	99.06 ± 1	98.67 ± 2	98.01 ± 2
6 nM scrambled	97.78 ± 2	99.24 ± 1	98.92 ± 1
8 nM scrambled	97.91 ± 3	98.46 ± 2	97.05 ± 3
10 nM scrambled	98.72 ± 2	97.88 ± 2	98.81 ± 2
2 nM siRNA	95.23 ± 2	93.87 ± 1	83.89 ± 3
4 nM siRNA	88.34 ± 2	85.89 ± 1*	82.11 ± 1*
6 nM siRNA	80.66 ± 1*	78.34 ± 1*	76.08 ± 1*
8 nM siRNA	76.22 ± 2*	71.88 ± 3*	68.83 ± 3*
10 nM siRNA	73.34 ± 3*	49.31 ± 1*	48.77 ± 2*

The effect of RNA interference on the percentage of cell viability was determined though an MTT test in human anaplastic human thyroid cancer cell line cultures (8305C) transfected with different concentrations (2, 4, 6, 8, and 10 nM) of scrambled control or siRNA-TfR1 for 24, 48, and 72 h. Results are expressed as the mean ± SD of the values of five separated experiments performed in triplicate. *$p < 0.05$ for differences versus controls.

Effect of the TfR1 Silencing Gene on the Apoptotic Pathway

To investigate the association between the TfR1 silencing gene and the resistance of the human thyroid cancer cell lines to apoptosis, we tested caspase-3 cleavage activity and DNA fragmentation. A significant increase in caspase-3 cleavage was found in the TfR1 silencing gene of FTC-133 and 8305C cell lines (Figures 7A and 7B). Figure 8 shows DNA fragmentation evaluated by a TUNEL (terminal deoxynucleotidyltransferase-mediated deoxyuridine triphosphate [dUTP] nick end labeling) test in FTC-133 (Figure 8A) and 8305C (Figure 8B) cell lines. A significant DNA fragmentation in the TfR1 silencing gene in both cell lines was observed (Figures 8Ab and 8Bd), when compared with the respective scrambled-treated ones (Figures 8Aa and 8Bb). The effect appeared more evident in the FTC-133 cell line.

These experiments indicate a good correlation between the inhibitory effect in the TfR1 silencing gene and apoptotic pathway activation.

DISCUSSION

Thyroid cancer is a human malignancy that represents approximately 1% of all cancers. Even if it is not so widely diffused, it comprises more than 90% of all endocrine cancers. For this reason preventive, accurate detection of thyroid cancer and a consequent appropriate treatment for this disease are very important in clinical practice.

One of the new biotechnological approaches, based on biological systems, uses computational techniques. Computational tools allow the identification of new entities in signaling cascades as biomarkers and promising targets for anticancer clinical therapy. The use of the computational method, based on the MapReduce approach, was capable of searching and suggesting possible ancestor nodes, non-trivial and trivial nodes able to modulate specific targets inside TfR1 signaling pathways. Importantly, the *in silico* approach allowed us to identify TP53 protein and NF-κB as modulator and downstream targets of TfR1 signaling. TfR1 is tightly linked with the ERK1/2 pathway, which is a key player in cellular iron acquisition, and may have a crucial role in cancer development. The therapeutic approach of selectively targeting activated kinases has proven to be of great value for the treatment of a variety of cancers. Mitogen-activated protein kinase (MAPK) can regulate apoptosis through specific phosphorylation of downstream mediators of apoptosis, including the tumor suppressor p53, linking cellular stress signaling and the regulation of p53 activity. Phosphorylation of p53 regulates its activity altering protein stability, interaction with co-activators, and transcription of target genes as part of the cellular response to cancer.

Apoptosis plays a fundamental role in cell development, growth, maturation, and differentiation in the process of carcinogenesis. The TfR1 silencing gene was able to progressively decrease cellular viability and the rate of cell growth of FTC-133 and 8305C human thyroid cancer cell lines, when compared with the respective control. Furthermore, the effect induced the activation of the apoptotic pathway as confirmed by caspase-3 cleavage and DNA fragmentation. These results demonstrated that TfR1 has a specific role in thyroid cancer cell apoptosis-inducing activity at the molecular level. We found that the TfR1 silencing gene was able to inhibit the ERK1/2 signaling pathway and c-Myc upregulation in the FTC-133 and 8305C human thyroid cancer cell lines. In addition, it is able to block cell cycle progression, inducing a significant increase of apoptotic pathway activation.

These data suggest that TfR1 might be crucial for rapid and transient activation of the ERK signaling pathway, which induces a deregulation of genes involved in the aberrant accumulation of intracellular free iron. The transient increases in c-Myc expression, induced by iron, could lead to a deregulation of genes involved in its incorporation and storage, resulting in the accumulation of intracellular free iron and oxidative stress.[28] Furthermore, c-Myc directly stimulates the expression of IRP-2, a protein whose degradation is enhanced by iron supplementation.[27] In conditions of elevated iron, physiological degradation of IRP-2 is generally counterbalanced by c-Myc-driven *de novo* synthesis, allowing IRP-2 to exert its post-transcriptional regulatory effects. Therefore, the effects of iron concentration variations are attenuated by IRP-mediated mRNA regulation, which contributes to maintain an equilibrium between iron uptake by TfR1 and iron storage by ferritin.[28]

The regulation of iron-related genes by c-Myc contributes to the increase in intracellular free iron, which is an essential step in c-Myc-induced cell transformation. In addition, proliferating cells that express high levels of c-Myc also display high levels of TfR1. Therefore, a correlation appears between c-Myc overexpression and high incorporation of iron. Furthermore, downregulation of H-ferritin gene expression is necessary for c-Myc to induce cell proliferation and transformation.[28] Consequently, c-Myc-mediated

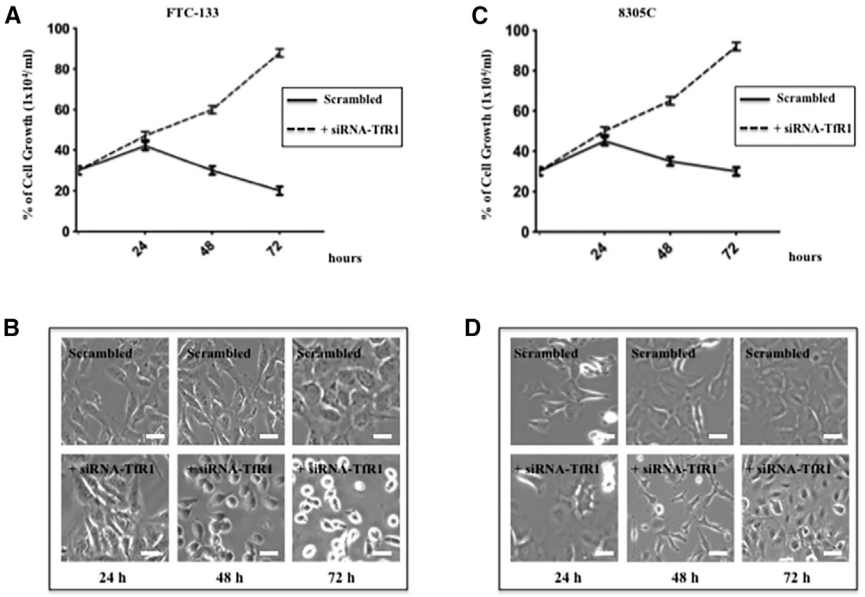

Figure 2. Effect of siRNA-TfR1 Transfection on Growth Curve and on Morphological Changes in FTC-133 and 8305C Cell Line Cultures

(A and C) FTC-133 (A) and 8305C (C) human thyroid cancer cell line proliferation rates through kinetics of cell growth curve analysis performed in 10 mM scrambled and siRNA-TfR1-transfected cells for 24, 48, and 72 h. Values represent the mean ± SD of five separate experiments performed in triplicate. *p < 005 versus scrambled cells used as a control. (B and D) Morphology evaluation of (B) FTC-133 and (D) 8305C cells. Morphological changes are apparent in FTC-133 and 8305C cells at 48 and 72 h. Magnification is equal in all images. Scale bars, 20 μm.

regulation of H-ferritin and IRP-2 can lead to additive effects that ultimately would increase the intracellular iron pool.

Taken together, i*n silico* and *in vitro* studies demonstrate that TfR1 plays a key role in human thyroid cancer and that its downregulation was able to inhibit ERK pathway, reducing also c-Myc expression, which activates the apoptotic pathway and blocks the cell cycle. These studies also suggest that TfR1 might be crucial for rapid and transient activation of the ERK signaling pathway, which induces a deregulation of genes involved in the aberrant accumulation of intracellular free iron. Thus, TfR1 might be an important target for thyroid cancer therapy, and further studies of this newly identified TfR1 signaling pathway are likely to provide insight into iron homeostasis in human thyroid cancer cells and its relationship to cancer cell survival and drug resistance.

MATERIALS AND METHODS

Materials

Follicular (FTC-133) and anaplastic (8305C) human thyroid cancer cells lines were obtained from the Cell Bank Interlab Cell Line Collection (Genoa, Italy). The media used for the cell culture included Dulbecco's modified Eagle's medium (DMEM) and minimum essential medium (MEM), containing 2 mM GlutaMAX (Gibco), Ham's F-12 (Gibco), non-essential amino acids, heat-inactivated fetal bovine serum (FBS, Gibco), normal goat serum (NGS, Gibco), streptomycin and penicillin solution, 0.05% trypsin-EDTA solution, mouse monoclonal antibody against TfR1, Lipofectamine 2000 transfection reagent, Opti-MEM I reduced serum media, Taq DNA polymerase, and glyceraldehyde-3-phosphate dehydrogenase (GAPDH) (from Invitrogen; Thermo Fisher Scientific, Milan, Italy). Chemically synthesized human transferrin receptor siRNA oligonucleotides and negative control scrambled siRNAs were from Ambion (Austin, TX, USA). A QIAGEN kit, aprotinin, leupeptin, pepstatin, phenylmethanesulfonylfluoride (PMSF), Lab-Tek chamber slides II, MTT, SYBR Green II, Triton X-100, dimethyl sulfoxide (DMSO), trypan blue solution, and other analytical chemicals were obtained from Sigma-Aldrich (Milano, Italy). Mouse monoclonal antibody against caspase-3 was from Becton Dickinson (Milan, Italy). Mouse monoclonal antibodies against p27, c-Myc, and β-tubulin were from Chemicon (Prodotti Gianni, Milan, Italy). Mouse monoclonal antibodies against p53, ERK1/2, and cyclin D_1 were from Abcam (Milan, Italy). Goat anti-mouse immunoglobulin G (IgG) peroxidase-conjugated secondary antibody, fluorescein isothiocyanate (FITC)-conjugated anti-mouse IgG polyclonal antibody, and tetramethylrhodamine isothiocyanate (TRITC)-conjugated anti-mouse IgG polyclonal antibody were from Chemicon (Prodotti Gianni, Milan, Italy). An ApoAlert DNA fragmentation assay kit was from Clontech (Milan, Italy). Horseradish peroxidase (HRP)-conjugated anti-mouse IgG was from Amersham Pharmacia Biotech (Milan, Italy). Mouse monoclonal antibody against Nestin as well as a Santa Cruz ECL (enhanced chemiluminescence) developing system for immunoblots were from Santa Cruz Biotechnology (Santa Cruz, CA, USA).

Methods

MapReduce Algorithm Approach

The approach based on a MapReduce algorithm was developed with the aim to scan and detect the signaling pathways collected into the KEGG database in order to discover trivial and non-trivial routes, starting from a specific target gene. The software has been developed for implementing the MapReduce algorithm through Python language and the mrjob library, while json and D3.js scripts were employed for the web interface. The mrjob library allows one to write MapReduce jobs in Python and run them in a platform-independent way. D3.js is a JavaScript library developed for visualizing data in a dynamic and interactive style starting from the use of organized numerical data. It combines HTML5, scalable vector graphics (SVG), and cascading style sheet (CSS) standards. The D3.js library allows the use of pre-built functions to select HTML document object model (DOM) elements, create SVG elements, according to predefined

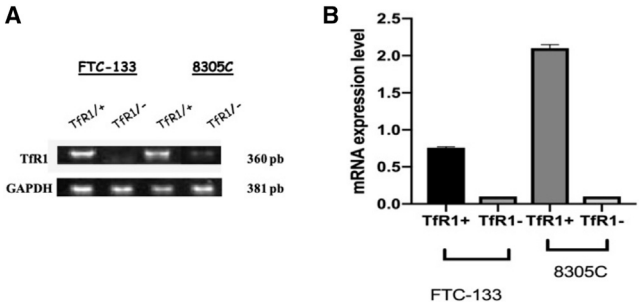

Figure 3. Effect of siRNA on mRNA Expression for TfR1 through Semiquantitative RT-PCR Analysis on FTC-133 and 8305C Cell Line Cultures

(A) Representative semiquantitative RT-PCR analysis for TfR1 mRNA expression in FTC-133 and 8305C human thyroid cancer cells lines scrambled (TfR1$^+$) and 10 nM siRNA-TfR1 transfected for 48 h (TfR1$^-$). (B) Densitometric analysis of RT-PCR products performed after normalization through using GAPDH as housekeeping gene. Results are expressed as the mean ± SD of the values of five separate experiments performed in triplicate. *$p < 0.05$ for differences versus controls.

graphical styles, and to add transitions and object movements. The software is presently accessible via http://combine.dmi.unict.it, where it can be easily tested. After execution of the software, through the calculate occurrence panel, it is possible to know the number of times a given path between the start and the end nodes has been found in all of the pathways downloaded from KEGG during the search process.

Cell Cultures

FTC-133 and 8305C cell lines, respectively, were cultured in DMEM supplemented with 2 mM Gluta-MAX, 10% FBS, and 50 μg/mL penicillin-streptomycin a final density of 2×10^6 cells and in Lab-Tek Chamber Slides II at a final density of 0.5×10^5 cells/well for the immunofluorescence assay.[29] Cells were cultured at 37°C in a humidified atmosphere of 5% CO_2. The medium was replaced every 2 or 3 days. At 85%–90% confluence, cells were suspended by using 0.05% trypsin and 0.53 mM EDTA solution for 5 min. Trypsinization was stopped by adding 20% FBS to the cell cultures. Cells were then centrifuged at $200 \times g$ for 10 min and the obtained pellets were suspended in the appropriate culture medium at a 1:4 density ratio, plated in 75-cm^2 flasks, in 96 multi-well, and in the 24 multi-well, in Lab-Tek Chamber Slides II, and incubated at 37°C in humidified 5% CO_2/95% air mixture.

Cell Transfection

siRNA transfections were performed at 35%–50% of confluence by using a BLOCK-iT transfection kit according to the manufacturer's instruction. FTC-133 and 8305C human thyroid cell lines were set up at density of 20×10^4 cells/well in 24-well plates in complete medium without antibiotics. Chemically synthesized human transferrin receptor siRNA oligonucleotides and negative control scrambled siRNA at different concentrations (2, 4, 6, 8, and 10 nM) and for different times (24, 48, and 72 h) were used. The target sequence for siRNA-TfR1 was 5′-AAC TTC AAG GTT TCT GCC AGC-3′. After transfection the culture medium was replaced with Opti-MEM supplemented with 1% (v/v) FBS. Cells were then incubated at 37°C in a humidified 5% CO_2/95% air mixture for 10–12 h. At the end of treatment time, the media were replaced with the media culture used.

MTT Bioassay

To monitor cell viability, FTC-133 and 8305C cell cultures were plated at a concentration of 60×10^4 cells/well (200 μL/well) on 96 multi-well flat-bottomed plates.[30] Cellular cytotoxicity was evaluated through use of an MTT reduction assay.[31] Briefly, MTT was added to each multi-well with a final concentration of 1.0 mg/mL, and cells were incubated at 37°C in a humidified 5% CO_2/95% air mixture for 1 h. After incubation with the reagent, the supernatant was removed and replaced with 200 μL of DMSO. The optical density of each well sample was measured with a microplate spectrophotometer reader (Titertek Multiskan; Flow Laboratories, Helsinki, Finland) at $\lambda = 570$ nm. The results were expressed as the percentage MTT reduction of control cells.

Cell Growth Curve

Cells in logarithmic phase growth were seeded at a concentration of 20×10^4 cells/well in a 24-well plate and transfected with 10 nM siRNA oligonucleotides and negative control scrambled siRNA. Following 24, 48, and 72 h the cells were harvested, diluted by trypan blue working solution and counted using a Burker chamber under a light microscope (Zeiss, Germany) to allow for growth curve construction. The cell growth curve was drawn according to the average cell number from each group.

Semiquantitative RT-PCR

Total RNA was isolated from FTC-133 and 8305C cell lines after siRNA-TfR1 using a QIAGEN kit. Five micrograms of RNA was reverse transcribed at 50°C for 1 h in a 20-mL reaction mix using the one-step ThermoScript RT-PCR following the manufacturer's instructions. PCR mixtures (100 μL) contained 5 mL of cDNA, 1× PCR buffer, 1.5 mM $MgCl_2$, 0.2 mM dNTP (2′-deoxynucleoside 5′-triphosphate), 1.25 U of Taq DNA polymerase, and 0.2 mM specific primers for TfR1. GAPDH-1, used for internal reaction control, was reverse transcribed with the following primers: sense, 5′-ACTCCC ATTCCTCCACCTTT-3′; antisense, 5′- TTACTCCTTGGAGGCCA TGT-3′. For each RT-PCR, a sample without reverse transcriptase was processed and used as a negative control. PCR conditions were set as follows: 1 cycle at 95°C for 3 min (reverse transcription); 25–35 cycles at 95°C for 1 min (denaturation of cDNA), 72°C for 1 min (annealing temperature), and a 72°C cycle for 7 min with an AmpliTaq PCR kit (PerkinElmer/Cetus Instruments, Norwalk, CT, USA). RT-PCR products were isolated on 2% agarose gel, by using SYBR Green II, and quantified by densitometric analysis with an AlphaImager 1200 system (Alpha Innotech, San Leandro, CA, USA).[32]

Immunocytochemical Procedures

Immunocytochemistry was performed to evaluate the expression of TfR1 on scrambled and 100 nM siRNA-TfR1-transfected FTC-133 and 8305C thyroid cancer cell lines for 48 h.[30,33] The cells were fixed with 4% paraformaldehyde for 15 min and then permeabilized with

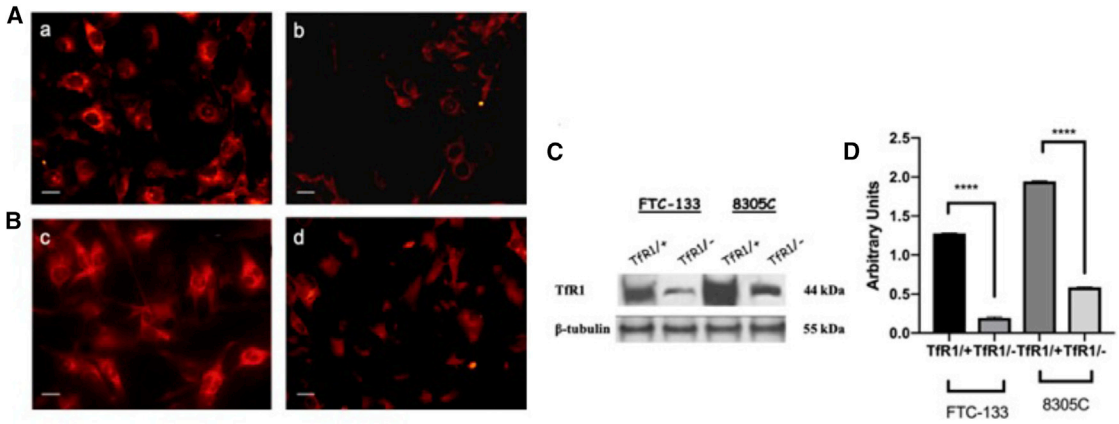

Figure 4. Effect of siRNA Gene Silencing on TfR1 Expression Levels through Immunofluorescence and Western Blotting Analysis on FTC-133 and 8305C Cell Line Cultures

(A) Positive immunofluorescence microscopic analysis for TfR1 in scrambled (a) FTC-133 and (c) 8305C human thyroid cancer cells lines and 10 nM siRNA-TfR1-transfected cells for 48 h. (b) FTC-133 and (d) 8305C human thyroid cancer cell lines. Magnification is equal in all images. Scale bars, 40 μm. (B) Representative immunoblot through western blotting analysis for TfR1 expression levels in total cellular lysates from scrambled and 10 nM siRNA-TfR1-transfected cells for 48 h. (C and D) Densitometric analysis of TfR1 expression (performed after normalization with β-tubulin) in both cell lines. Results are expressed as the mean ± SD of the values of five separate experiments performed in triplicate. *p < 0.05 for differences versus controls.

0.1% Triton X-100 in PBS for 10 minutes and then incubated overnight in the mouse monoclonal antibody against TfR1 (1:1,000). Subsequently, coverslips were treated with secondary antibody, goat anti-mouse antibody IgG, and fluorescein isothiocyanate (FITC, 1:100). Coverslips were washed, mounted in PBS/glycerol (50:50), placed on glass microscope slides, and analyzed on a fluorescence microscope (Leica, Germany). No non-specific staining of FTC-133 and 8305C cell lines cultures was observed in control incubations in which the primary antibody was omitted.

Western Blotting Analysis

FTC-133 and 8305C thyroid cancer cell lines for all of our experimental conditions were collected in cold PBS, isolated by centrifugation, and resuspended in a homogenizing buffer containing

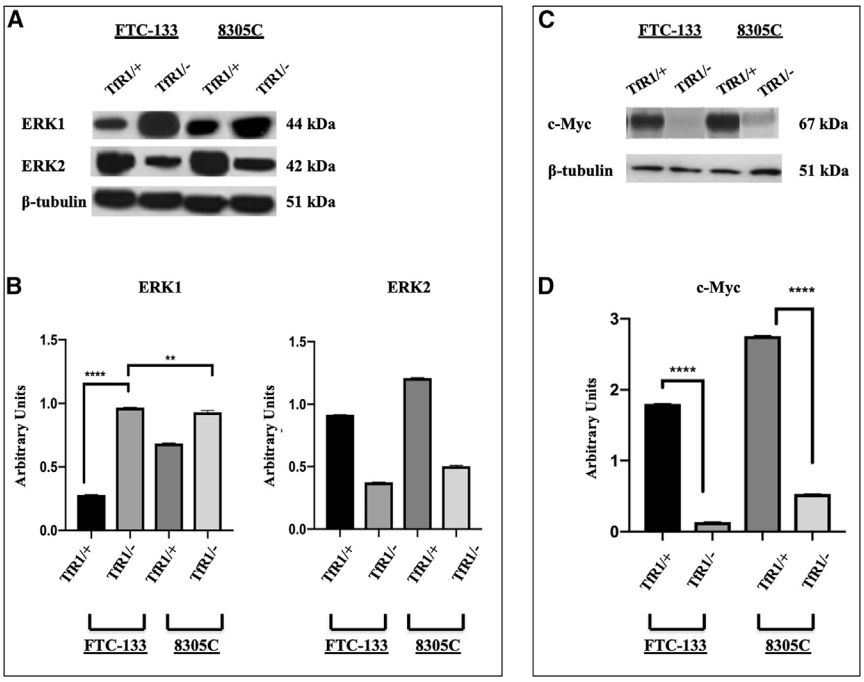

Figure 5. Effect of siRNA Gene Silencing on ERK1/2 Pathway through Western Blotting Analysis on FTC-133 and 8305C Cell Line Cultures

(A) Representative immunoblots of ERK1/2 expression levels in total cellular lysates from scrambled FTC-133 and 8305C human thyroid cancer cell lines and 10 nM siRNA-TfR1-transfected cells for 48 h. (B) Densitometric analysis of ERK1 and ERK2 expression levels in response to siRNA-TfR1 gene silencing in transfected FTC-133 and 8305 human thyroid cancer cell lines, when compared with scrambled ones, used as control (performed after normalization with β-tubulin). (C) Representative immunoblot of c-Myc expression levels in total cellular lysates from scrambled FTC-133 and 8305C human thyroid cancer cell lines and 10 nM siRNA-TfR1 transfected cells for 48 h. (D) Densitometric analysis of c-Myc (performed after normalization with β-tubulin) in response to siRNA-TfR1 transfection, when compared with scrambled ones, used as control. Results are expressed as the mean ± SD of the values of five separate experiments performed in triplicate. *p < 0.05 for differences versus controls.

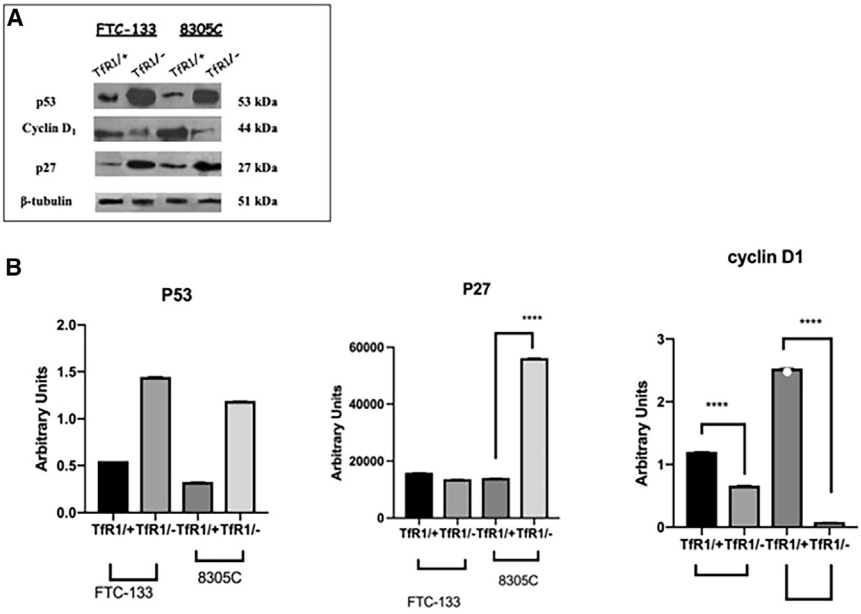

Figure 6. Effect of siRNA Gene Silencing on p53, p27, and cyclin D_1 Expression Levels through Western Blotting Analysis on FTC-133 and 8305C Cell Line Cultures

(A) Representative immunoblots of p53, p27, and cyclin D_1 expression levels in total cellular lysates from scrambled FTC-133 and 8305C human thyroid cancer cell lines and 10 nM siRNA-TfR1-transfected cells for 48 h. (B) Densitometric analysis of p53, cyclin D_1, and p27 (performed after normalization with β-tubulin) in response to siRNA-TfR1 transfection, when compared with scrambled ones, used as control. Results are expressed as the mean ± SD of the values of five separate experiments performed in triplicate. *p < 0.05 for differences versus controls.

50 mM Tris-HCl (pH 6.8), 150 mM NaCl, 1 mM EDTA, and 0.1 mM PMSF supplemented with 10 μg/mL aprotinin, leupeptin, and pepstatin and then sonicated on ice.[32–34] Briefly, the protein concentration of the homogenates was then diluted to 1 mg/mL with reducing stop buffer (0.25 M Tris-HCl, 5 mM EGTA, 25 mM dithiothreitol, 2% SDS, and 10% glycerol with bromophenol blue as the tracking dye).[30,32] Proteins were separated on 10% SDS-polyacrylamide gels and transferred to nitrocellulose membranes. Blots were blocked overnight at 4°C with 5% non-fat dry milk dissolved in 20 mM Tris-HCl (pH 7.4), 150 mM NaCl, and 0.5% Tween 20, and then the samples were probed with appropriate antibodies against TfR1, caspase-3, p53, p27, cyclin D_1, ERK1/2, c-Myc, and β-tubulin (1:1,000 in PBS). Blots were then scanned and quantified with an AlphaImager 1200 system (Alpha Innotech, San Leandro, CA, USA). The expression of each protein was visualized with an ECL kit after autoradiography film exposure. Blots were then scanned and quantified with an AlphaImager 1200 System (Alpha Innotech, San Leandro, CA, USA). Densitometric analysis was performed after normalization with anti-rabbit β-tubulin.

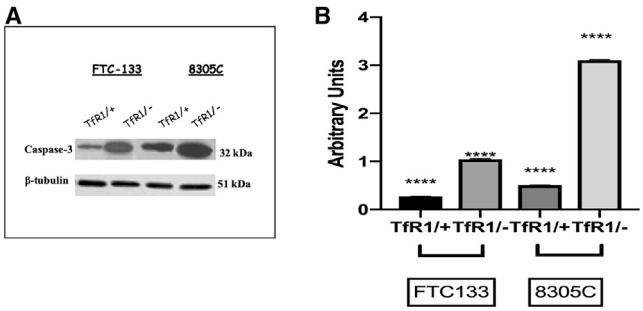

Figure 7. Effect of siRNA Gene Silencing on Caspase-3 Cleavage through Western Blotting Analysis on FTC-133 and 8305C Cell Line Cultures

(A) Representative immunoblot of caspase-3 cleavage in total cellular lysates from scrambled FTC-133 and 8305C human thyroid cancer cell lines and 10 nM siRNA-TfR1 transfected cells for 48 h. (B) Densitometric analysis of caspase-3 (performed after normalization with β-tubulin) in response to siRNA-TfR1 transfection, when compared with scrambled ones, used as control. Results are expressed as the mean ± SD of the values of five separate experiments performed in triplicate. *p < 0.05 for differences versus controls.

TUNEL Test

To assess DNA nuclear fragmentation an ApoAlert DNA kit was used. The ApoAlert DNA fragmentation assay incorporates fluorescein-dUTP at the free 3′-hydroxyl ends of the fragmented DNA using TUNEL and was performed according to the user's manual. FTC-133 and 8305C cell cultures, scrambled and 10 nM siRNA-TfR1-transfected FTC-133 and 8305C cell cultures for 48 h were made up according to the user's manual. Cells were mounted and visualized directly by fluorescence microscopy (Leica, Germany) with either a propidium iodide (PI) filter alone or a FITC filter alone. According to the user's manual, apoptotic cells appear green with the FITC filter alone whereas non-apoptotic cells appear red under the dual-pass FITC/PI filter set. We focused on 10 random microscopic fields for each dish. In each microscopic field, the number of apoptotic cells is counted and this number is compared with the number of all non-apoptotic cells visualized in the same microscopic field. The ratio is expressed as a percentage.[29]

Statistical Analysis

Data were statistically analyzed using one-way analysis of variance (ANOVA) followed by a *post hoc* Holm-Sidak test to estimate significant differences among groups. Data were reported as mean ± SD of five separated experiments performed in triplicate, and differences between groups were considered to be significant at *p <0.05.

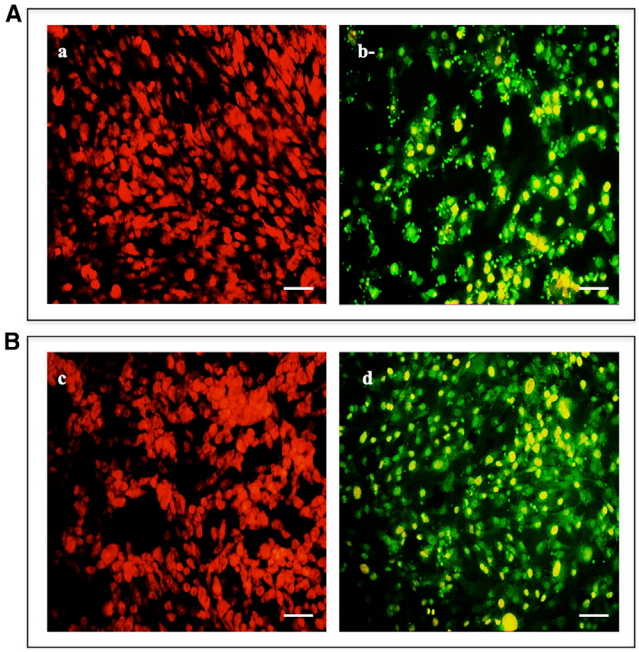

Figure 8. Effect of siRNA Gene Silencing on DNA Fragmentation through TUNEL Test on FTC-133 and 8305C Cell Line Cultures

(A and B) Representative images of TUNEL assay performed in (A) FTC-133 and (B) 8305C human thyroid cancer cell lines scrambled (a and c) and 10 nM siRNA-TfR1-transfected cells for 48 h (b and d). Immunostaining of non-apoptotic (red) and apoptotic (green) cells is shown. Magnification is equal in all images. Scale bars, 20 μm.

AUTHOR CONTRIBUTIONS

A.C. conceived this project and wrote the manuscript with the approval of all authors; R.B. carried out the experiments; G.R., G.M., and R.P. supervised the project; G.B. processed the experimental data and aided in interpreting the results; F.P. conceived, designed, and supervised the computational study; G.R. and M.P. performed the computational simulations and analyzed the *in silico* data; M.A.C. and L.L. collaborated on computational simulations and the analysis of the *in silico* data. All authors discussed the results and contributed to the final draft of the manuscript.

ACKNOWLEDGMENTS

The authors acknowledge PRIN MIUR 2008 (code 2008XAWB9H_003) as partially supporting the research.

REFERENCES

1. van Staveren, W.C.G., Solís, D.W., Delys, L., Duprez, L., Andry, G., Franc, B., Thomas, G., Libert, F., Dumont, J.E., Detours, V., and Maenhaut, C. (2007). Human thyroid tumor cell lines derived from different tumor types present a common dedifferentiated phenotype. Cancer Res. *67*, 8113–8120.

2. Anabousi, S., Bakowsky, U., Schneider, M., Huwer, H., Lehr, C.M., and Ehrhardt, C. (2006). *In vitro* assessment of transferrin-conjugated liposomes as drug delivery systems for inhalation therapy of lung cancer. Eur. J. Pharm. Sci. *29*, 367–374.

3. Chiotoglou, I., Smilevska, T., Samara, M., Likousi, S., Belessi, C., Athanasiadou, I., Stavroyianni, N., Samara, S., Laoutaris, N., Vamvakopoulos, N., et al. (2008). Predominantly post-transcriptional regulation of activation molecules in chronic lymphocytic leukemia: the case of transferrin receptors. Blood Cells Mol. Dis. *41*, 203–209.

4. Beguin, Y., Yerna, M., Loo, M., Weber, M., and Fillet, G. (1992). Erythropoiesis in multiple myeloma: defective red cell production due to inappropriate erythropoietin production. Br. J. Haematol. *82*, 648–653.

5. Hartford, T., O'Brien, S., Andrew, P.W., Jones, D., and Roberts, I.S. (1993). Utilization of transferrin-bound iron by *Listeria monocytogenes*. FEMS Microbiol. Lett. *108*, 311–318.

6. Lawrence, C.M., Ray, S., Babyonyshev, M., Galluser, R., Borhani, D.W., and Harrison, S.C. (1999). Crystal structure of the ectodomain of human transferrin receptor. Science *286*, 779–782.

7. Bennett, M.J., Lebrón, J.A., and Bjorkman, P.J. (2000). Crystal structure of the hereditary haemochromatosis protein HFE complexed with transferrin receptor. Nature *403*, 46–53.

8. Rao, K.K., Shapiro, D., Mattia, E., Bridges, K., and Klausner, R. (1985). Effects of alterations in cellular iron on biosynthesis of the transferrin receptor in K562 cells. Mol. Cell. Biol. *5*, 595–600.

9. Cheng, Y., Zak, O., Aisen, P., Harrison, S.C., and Walz, T. (2004). Structure of the human transferrin receptor-transferrin complex. Cell *116*, 565–576.

10. Bianchi, L., Tacchini, L., and Cairo, G. (1999). HIF-1-mediated activation of transferrin receptor gene transcription by iron chelation. Nucleic Acids Res. *27*, 4223–4227.

11. Klausner, R.D., Rouault, T.A., and Harford, J.B. (1993). Regulating the fate of mRNA: the control of cellular iron metabolism. Cell *72*, 19–28.

12. Hentze, M.W., and Kühn, L.C. (1996). Molecular control of vertebrate iron metabolism: mRNA-based regulatory circuits operated by iron, nitric oxide, and oxidative stress. Proc. Natl. Acad. Sci. USA *93*, 8175–8182.

13. Hsing, A.W., McLaughlin, J.K., Olsen, J.H., Mellemkjar, L., Wacholder, S., and Fraumeni, J.F., Jr. (1995). Cancer risk following primary hemochromatosis: a population-based cohort study in Denmark. Int. J. Cancer *60*, 160–162.

14. Goldstein, S.R., Yang, G.Y., Chen, X., Curtis, S.K., and Yang, C.S. (1998). Studies of iron deposits, inducible nitric oxide synthase and nitrotyrosine in a rat model for esophageal adenocarcinoma. Carcinogenesis *19*, 1445–1449.

15. Chen, X., Yang, Gy., Ding, W.Y., Bondoc, F., Curtis, S.K., and Yang, C.S. (1999). An esophagogastroduodenal anastomosis model for esophageal adenocarcinogenesis in rats and enhancement by iron overload. Carcinogenesis *20*, 1801–1808.

16. Chen, X., and Yang, C.S. (2001). Esophageal adenocarcinoma: a review and perspectives on the mechanism of carcinogenesis and chemoprevention. Carcinogenesis *22*, 1119–1129.

17. Miskimins, W.K., Roberts, M.P., McClelland, A., and Ruddle, F.H. (1985). Use of a protein-blotting procedure and a specific DNA probe to identify nuclear proteins that recognize the promoter region of the transferrin receptor gene. Proc. Natl. Acad. Sci. USA *82*, 6741–6744.

18. Testa, U., Pelosi, E., and Peschle, C. (1993). The transferrin receptor. Crit. Rev. Oncog. *4*, 241–276.

19. Cavanaugh, P.G. (2002). Synthesis of chlorin e6-transferrin and demonstration of its light-dependent in vitro breast cancer cell killing ability. Breast Cancer Res. Treat. *72*, 117–130.

20. O'Donnell, K.A., Yu, D., Zeller, K.I., Kim, J.W., Racke, F., Thomas-Tikhonenko, A., and Dang, C.V. (2006). Activation of transferrin receptor 1 by c-Myc enhances cellular proliferation and tumorigenesis. Mol. Cell. Biol. *26*, 2373–2386.

21. Iritani, B.M., and Eisenman, R.N. (1999). c-Myc enhances protein synthesis and cell size during B lymphocyte development. Proc. Natl. Acad. Sci. USA *96*, 13180–13185.

22. Kasibhatla, S., Jessen, K.A., Maliartchouk, S., Wang, J.Y., English, N.M., Drewe, J., Qiu, L., Archer, S.P., Ponce, A.E., Sirisoma, N., et al. (2005). A role for transferrin receptor in triggering apoptosis when targeted with gambogic acid. Proc. Natl. Acad. Sci. USA *102*, 12095–12100.

23. Xing, M., Usadel, H., Cohen, Y., Tokumaru, Y., Guo, Z., Westra, W.B., Tong, B.C., Tallini, G., Udelsman, R., Califano, J.A., et al. (2003). Methylation of the thyroid-stimulating hormone receptor gene in epithelial thyroid tumors: a marker of malignancy and a cause of gene silencing. Cancer Res. *63*, 2316–2321.

24. Stenner, F., Liewen, H., Zweifel, M., Weber, A., Tchinda, J., Bode, B., Samaras, P., Bauer, S., Knuth, A., and Renner, C. (2008). Targeted therapeutic approach for an anaplastic thyroid cancer *in vitro* and *in vivo*. Cancer Sci. *99*, 1847–1852.

25. Wang, P.P., Ma, L., Lv, Y.H., Xiang, Y., Shao, D.G., Sun, R., Yang, S.H., and Hu, R. (2017). [The efficacy of thyroid hormone replacement therapy in patients with hypothyroidism and OSAHS: a meta analysis]. Lin Chung Er Bi Yan Hou Tou Jing Wai Ke Za Zhi *31*, 1362–1366.

26. Gianì, F., Russo, G., Pennisi, M., Sciacca, L., Frasca, F., and Pappalardo, F. (2019). Computational modeling reveals MAP3K8 as mediator of resistance to vemurafenib in thyroid cancer stem cells. Bioinformatics *35*, 2267–2275.

27. Cairo, G., and Pietrangelo, A. (2000). Iron regulatory proteins in pathobiology. Biochem. J. *352*, 241–250.

28. Habel, M.E., and Jung, D. (2006). Free radicals act as effectors in the growth inhibition and apoptosis of iron-treated Burkitt's lymphoma cells. Free Radic. Res. *40*, 789–797.

29. Chiacchio, U., Barbera, V., Bonfanti, R., Broggini, G.L., Campisi, A., Gazzola, S., Parenti, R., and Romeo, G. (2013). Synthesis and biological evaluation of 1,7,8,8a-tetrahydro-3*H*-oxazolo[3,4-a]pyrazin-6(5*H*)-ones as antitumoral agents. Bioorg. Med. Chem. *21*, 5748–5753.

30. Campisi, A., Caccamo, D., Raciti, G., Cannavò, G., Macaione, V., Currò, M., Macaione, S., Vanella, A., and Ientile, R. (2003). Glutamate-induced increases in transglutaminase activity in primary cultures of astroglial cells. Brain Res. *978*, 24–30.

31. Mosmann, T. (1983). Rapid colorimetric assay for cellular growth and survival: application to proliferation and cytotoxicity assays. J. Immunol. Methods *65*, 55–63.

32. Campisi, A., Caccamo, D., Li Volti, G., Currò, M., Parisi, G., Avola, R., Vanella, A., and Ientile, R. (2004). Glutamate-evoked redox state alterations are involved in tissue transglutaminase upregulation in primary astrocyte cultures. FEBS Lett. *578*, 80–84.

33. Campisi, A., Spatuzza, M., Russo, A., Raciti, G., Vanella, A., Stanzani, S., and Pellitteri, R. (2012). Expression of tissue transglutaminase on primary olfactory ensheathing cells cultures exposed to stress conditions. Neurosci. Res. *72*, 289–295.

34. Campisi, A., Gulino, M., Acquaviva, R., Bellia, P., Raciti, G., Grasso, R., Musumeci, F., Vanella, A., and Triglia, A. (2010). Reactive oxygen species levels and DNA fragmentation on astrocytes in primary culture after acute exposure to low intensity microwave electromagnetic field. Neurosci. Lett. *473*, 52–55.